Pramana – J. Phys. (2019) 93:25
https://doi.org/10.1007/s12043-019-1772-9

Tunnel magnetoresistance in the $B_nN_n(n = 12, 24)$ cages

YAGHOOB MOHAMMADMORADI and MOJTABA YAGHOBI*

Ayatollah Amoli Branch, Islamic Azad University, 602 Amol, Iran
*Corresponding author. E-mail: m.yaghoubi@iauamol.ac.ir

MS received 7 August 2018; revised 9 December 2018; accepted 4 January 2019; published online 23 May 2019

Abstract. In this study, the effects of the type of the cage, the bias and gate voltages on spin transport properties of electrons in magnetic tunnel junction (MTJ) of $B_nN_n(n = 12, 24)$ cages were investigated by theoretical methods. For a gate voltage (V_g) more than 0.5 V, the device became electrically conductive at $V_b = 0.5$ V. The electric current increased linearly for bias voltages more than $|V_b| = 1$ V at $V_g = 0.0$ V. The maximum value of the tunnel magnetic resistance (TMR) ratio was ∼75% for $B_{12}N_{12}$ and 60% for $B_{24}N_{24}$ molecules. The maximum values of TMR against the bias voltage (V_b) were seen at 1.6 V (−1.6 V) for $B_{12}N_{12}$ and 0.0 V for $B_{24}N_{24}$. At $V_b = 0.5$ V, the TMR ratio was changed by varying the gate voltage. Finally, the spin transport properties of the $B_{12}N_{12}$ cage were compared with those of the $B_{24}N_{24}$ and C_{60} cages.

Keywords. Spin-dependent transport; tunnelling magnetoresistance; fullerene-like alternate BN cages; non-equilibrium Green's function.

PACS Nos 31.15.Bu; 72.10.Bg; 85.75.–d; 85.35.Gv

1. Introduction

The spin transport electronics is useful in many studies and industry fields such as very sensible sensors and magnetoresistive random access memory (MRAM) devices [1–18]. A thin insulating barrier layer squeezed between two ferromagnetic metal layers is called a magnetic tunnel junction (MTJ). In the MTJ, the direction of the tunnelling current is different from the direction of the magnetic field in two ferromagnetic metal layers. This effect is referred to as tunnel magnetic resistance (TMR). The TMR effects can be seen in systems with spin-polarised transport, such as single and multiwalled carbon nanotubes, semiconductor quantum dots connected by a molecular bridge, organic thin films and self-assembled organic monolayers [2,7].

For the first time, in 1975, Jullière [8] found the TMR effect in Fe/Ge–O/Co junctions. The reported values of TMR were small at 4.2 K temperature. Thus, they did not have any application in the fields of industry. In another work, Miyazaki and Tezuka [9] found large values of TMR. Moodera *et al* [10] worked on a new fabrication process in order to fulfil the smooth and the pinhole-free Al_2O_3 deposition.

According to the experimental works conducted in this field, the organic molecules show a large TMR [3–20]. At low bias voltages, Zare-Kolsaraki and Micklitz [15] reported that the maximum TMR ratio of C_{60}−Co composite is ∼30%. Using the single-band tight-binding approximation, the maximum TMR ratio (more than 60%) was obtained at low bias voltages ($V_b < 0.2$ V) for C_{60} [16].

In addition, theories predicted that the spin–orbit interaction and spin-flip scattering are generally negligible in organic molecular systems. It is an important advantage for applications in molecular spintronics [4]. It has been shown that the magnitude and sign of TMR can change for various barrier materials [12]. For a single C_{60} molecule inserted between two ferromagnetic Ni leads, the TMR values can reach −80% [17]. The TMR ratios higher than −60% were obtained for Co/C_{60}/Co/Ni junctions. In addition, a change in TMR from −63 to −94% was reported in [18].

The effect of temperature on the resistive and giant magnetoresistance was investigated in [12,13].

Because of the perfect symmetrical structure, shape and electronic properties, the B–N cages have attracted the attention of researchers [14–22]. Using the Hartree–Fock and density functional theories, Strout [19] investigated the isomers of $B_{12}N_{12}$. In an experimental work, Stéphan *et al* [20] indicated that the diameters of the B–N cages change from 0.4 to 0.7 nm. The B–N cages can be made by square, hexagonal and octagonal rings with alternate B and N atoms [20–22].

Electron transport through BN structures was studied [23–27] in recent years. Gupta *et al* [24] investigated the properties of the spin-polarised transport of the doped BN monolayers. The spin-polarised electron transport of BN nanoribbons was investigated using theoretical methods [26]. Photoluminescence, Coulomb blockade and supermagnetism properties were seen in the studies related to B–N materials [28].

2. Method

Figure 1 shows the geometry of the magnetic junction when a $B_nN_n (n = 12, 24)$ molecule is attached between two semi-infinite ferromagnetic electrodes.

The Hamiltonian of such a system can be shown as

$$\hat{H} = \hat{H}_{\mathrm{C}} + \sum_{\alpha=\mathrm{L,R}} (H_\alpha + H_{\alpha\mathrm{C}}) \quad (\alpha = \mathrm{L,R}). \tag{1}$$

Using the approximation of tight binding, the Hamiltonians of ferromagnetic (FM) electrodes can be described as

$$\hat{H}_\alpha = \sum_{(i_\alpha, j_\alpha),\sigma} (\varepsilon_{\alpha,\sigma}\delta_{i_\alpha,j_\alpha} - t_{i_\alpha,j_\alpha}) c^+_{i_\alpha,\sigma} c_{j_\alpha,\sigma} \quad (\alpha = \mathrm{L,R}), \tag{2}$$

where for the nearest adjacent atoms, the hopping integral t_{i_α,j_α} is equal to t_0. In eq. (2), we have $\varepsilon_{\alpha,\sigma} = \varepsilon_0 - \sigma \cdot h_\alpha$, where the on-site energy (ε_0) of the electrode is considered to be equal to $3t_0$. Moreover, h_α and $-\sigma \cdot h_\alpha$ denote the molecular field and the internal exchanged energy, respectively. For the site i of electrode α, the creation (annihilation) operator of an electron is shown as $c^+_{i\alpha,\sigma}(c_{i\alpha,\sigma})$.

Saffarzadeh [16] showed which bond dimerisation could affect the electron transmission characteristics. Therefore, the hopping strength ($t_{i,j}$) in the B_nN_n molecule depends on the B–N bond length that is calculated using the Su–Schrieffer–Heeger (SSH) model [29]. The channel Hamiltonian when the FM electrodes do not exist can be described using the following Hamiltonian [29,30]:

$$\hat{H}_{\mathrm{C}} = \sum_i \varepsilon_{\mathrm{C}} d^+_{i\mathrm{C},\sigma} d_{i\mathrm{C},\sigma} + H^{(0)}_{\mathrm{B-N}}, \tag{3}$$

$$H^{(0)}_{\mathrm{B-N}} = \sum_{\langle i,j\rangle} \sum_\sigma \left[-t_0 - \alpha_0 y_{i,j}\right](d^+_{i\mathrm{C},\sigma} d_{j\mathrm{C},\sigma} + \mathrm{h.c.}) + \frac{1}{2}\sum_{\langle i,j\rangle} K_0 (y_{ij})^2, \tag{4}$$

where for site i of B_nN_n molecule, the creation (annihilation) operator of an electron is shown as $d^+_{i\mathrm{C},\sigma}(d_{i\mathrm{C},\sigma})$, the gate voltage is effective by the on-site energy of the channel (ε_{C}), α_0 and y_{ij} are the electron–lattice weak coupling constant for the B–N bonds and the change in bond length between the ith and jth atoms, respectively, and K_0 denotes the spring constant related to the B–N bonds.

Finally, the influence between the channel and FM leads is written as

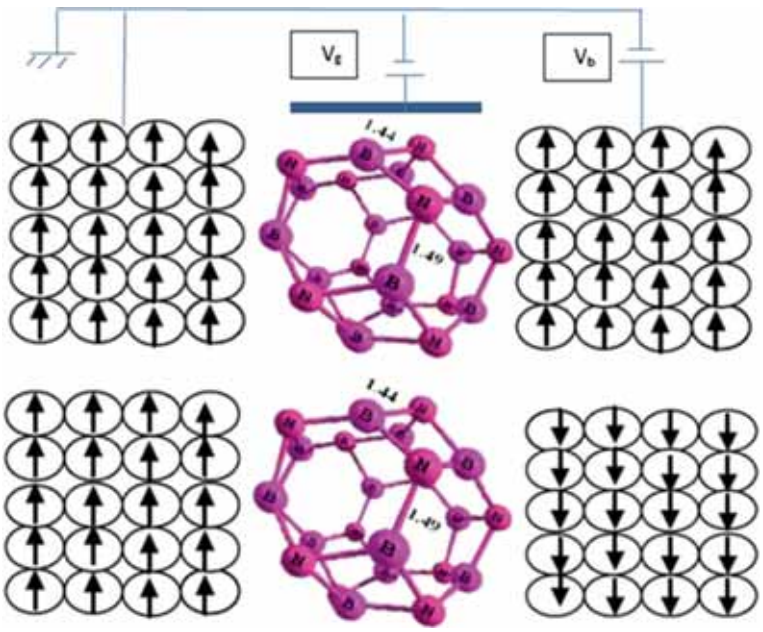

Figure 1. Schematic view of the $FM/B_{12}N_{12}/FM$ molecular junction. The insulator between the gate terminal and the molecule should be thin enough so that the gate voltage can control the electron density in the channel.

$$\hat{H}_{\alpha\mathrm{C}} = \sum_{\alpha=\{\mathrm{L,R}\}} \sum_{(i_\alpha, j_c),\sigma} (-t_{i_\alpha, j_c})(c^{+}_{i_\alpha,\sigma} d_{j_c,\sigma} + \mathrm{h.c.}), \tag{5}$$

where $t_{i_\alpha, j_c} = t'$ is the hopping element between the sites i of the lead α and the sites j of the molecule. The transport is supposed to be ballistic and the resistance comes from the contacts. The effect of spin-flip scattering is ignored in calculations because the diameter of the organic molecules is smaller than their length of spin diffusion [28]. Therefore, the Landauer formula is applied to estimate the spin-dependent electric current [30,31], which is given as follows:

$$I^{\sigma}(V_\mathrm{b}, V_\mathrm{g}) = \frac{e}{h} \int_{\mu_\mathrm{R}}^{\mu_\mathrm{L}} [f(\varepsilon - \mu_\mathrm{L}) - f(\varepsilon - \mu_\mathrm{R})] \times T^{\sigma}(\varepsilon, V_\mathrm{b}, V_\mathrm{g})\, \mathrm{d}\varepsilon, \tag{6}$$

where $\mu_\alpha = E_f \pm (1/2)eV_\mathrm{b}$ is the electrochemical potential of the electrode α, h is the Planck's constant, e represents the electron charge and f denotes the Fermi distribution function.

The spin-dependent transmission function of the system $T^{\sigma}(\varepsilon, V_\mathrm{b}, V_\mathrm{g})$ at an energy level ε and under the external V_b (bias voltage) and V_g (gate voltage) can be calculated by the non-equilibrium Greens function (NEGF) method as [31]

$$T^{\sigma}(\varepsilon, V_\mathrm{b}, V_\mathrm{g}) = \mathrm{Tr}[\Gamma_\mathrm{L}(\varepsilon - eV_\mathrm{b}/2) G^{\mathrm{r}}_{\mathrm{C},\sigma}(\varepsilon, V_\mathrm{b}, V_\mathrm{g}) \times \Gamma_\mathrm{R}(\varepsilon + eV_\mathrm{b}/2) G^{\mathrm{a}}_{\mathrm{C},\sigma}(\varepsilon, V_\mathrm{b}, V_\mathrm{g})]. \tag{7}$$

In the above equation, the Green's function of retarded (advanced) is indicated as $G^{\mathrm{r(a)}}_{\mathrm{C},\sigma}$ with σ spin. Under the external V_b and V_g, the Green's function, the coupling functions Γ_α and the self-energy matrix ($\Sigma_{\mathrm{L},\sigma}$) for the lead α are defined as follows:

$$G_{\mathrm{C},\sigma}(\varepsilon, V_\mathrm{b}, V_\mathrm{g}) = [\varepsilon \hat{I} - H_\mathrm{C}(V_\mathrm{g}) - \Sigma_{\mathrm{L},\sigma}(\varepsilon + eV_\mathrm{b}/2) - \Sigma_{\mathrm{R},\sigma}(\varepsilon - eV_\mathrm{b}/2)]^{-1}, \tag{8}$$

$$\Sigma_{\alpha,\sigma}(\varepsilon) = \hat{\tau}_{\mathrm{C},\alpha} \hat{g}_{\alpha,\sigma}(\varepsilon) \hat{\tau}_{\alpha,\mathrm{C}} \quad (\alpha = \mathrm{L,R}), \tag{9}$$

$$\Gamma_\alpha(\varepsilon) = -2\,\mathrm{Im}\,\Sigma_{\alpha,\sigma}(\varepsilon), \tag{10}$$

where the elements of the matrix $\hat{\tau}_{\mathrm{C},\alpha}$ are the hopping strength between the lead α and the molecule. In addition, the surface Green's function ($g_{\alpha,\sigma}$) is calculated by applying the Lehman method for the uncoupled FM electrodes [30,32]. Their matrix elements are given by

$$\big(g_{\alpha,\sigma}(z = \varepsilon + \mathrm{i}\delta)\big)_{ij} = \sum_k \frac{\varphi_k(r_i)\, \varphi^{*}_k(r_j)}{z - \varepsilon_0 + \sigma \cdot h_\alpha + \varepsilon(\mathbf{k})}, \tag{11}$$

where $\mathbf{k} \equiv (l_x, l_y, k_z)$ and $z = \varepsilon + \mathrm{i}\delta$.

$$\varphi_k(r_i) = \frac{2\sqrt{2}}{\sqrt{(N_x+1)\,(N_y+1)N_z}} \times \sin\left(\frac{l_x x_i \pi}{N_x+1}\right) \sin\left(\frac{l_y y_i \pi}{N_y+1}\right) \sin(k_z z_i), \tag{12}$$

$$\varepsilon(\mathbf{k}) = 2t\left[\cos\left(\frac{l_x \pi}{N_x+1}\right) + \cos\left(\frac{l_y \pi}{N_y+1}\right) + \cos(k_z a)\right]. \tag{13}$$

Here, $l_{x\cdot y}\,(=1, \ldots, N_{x\cdot y})$ are integers, $k_z \in [-(\pi/a), (\pi/a)]$ and N_β with $\beta = x, y, z$ are the number of the lattice sites in the β direction. The Green's function is estimated by considering a convergence of change in the bond lengths [33].

The TMR ratio can be calculated from the following general definition:

$$\mathrm{TMR} = \frac{I_\mathrm{p} - I_\mathrm{a}}{I_\mathrm{p}}, \tag{14}$$

where the total currents in the parallel and antiparallel alignments of the magnetisations in the leads are presented as I_p and I_a, respectively.

3. Results and discussion

The spin-dependent transport and TMR effect of $B_{12}N_{12}$ and $B_{24}N_{24}$ molecules are investigated using the method described in §2. The leads and the B_nN_n molecules are taken symmetrically with regard to the plane passing through the centre of mass of the molecule. When the molecule is brought close to an electrode, B_nN_n molecule ($n = 12, 24$) can be coupled through one atom to a central atom of each lead [16]. We fix magnetisation in the $+y$ direction of the left electrode, whereas it can change in the $+y$ and $-y$ directions of the right electrode. The optimised structures of $B_{12}N_{12}$ and $B_{24}N_{24}$ molecules are displayed in figures 2a and 2b, respectively. The $B_{12}N_{12}$ clusters consist of four- and six-ring BNs with T_h symmetry [34,35].

The $B_{24}N_{24}$ molecule consists of 12 tetragonal, 8 hexagonal and 6 octagonal BN rings with the O symmetry [36]. Proportional to the energy gap and bond lengths of B_nN_n molecule, we selected the values of the parameters as $t_0 = 3.1$ eV, $t' = 0.5\,t_0$, $\alpha = 6$ eV/Å, $h_\alpha = 4.5$ eV, $T = 300$ K, $N_x = N_y = 5$ and $K = 250.0$ eV/A^2 [37].

The band gap is an important factor in the properties of the transport through molecular junctions. The degeneracy of $B_{12}N_{12}$ and $B_{24}N_{24}$ molecules is traced as a function of energy in figures 3a and 3b,

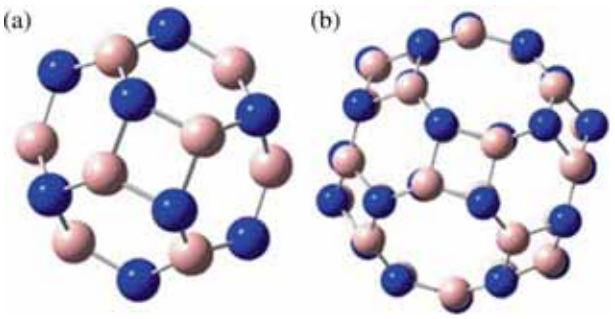

Figure 2. The optimised structure of (**a**) $B_{12}N_{12}$ and (**b**) $B_{24}N_{24}$ molecules.

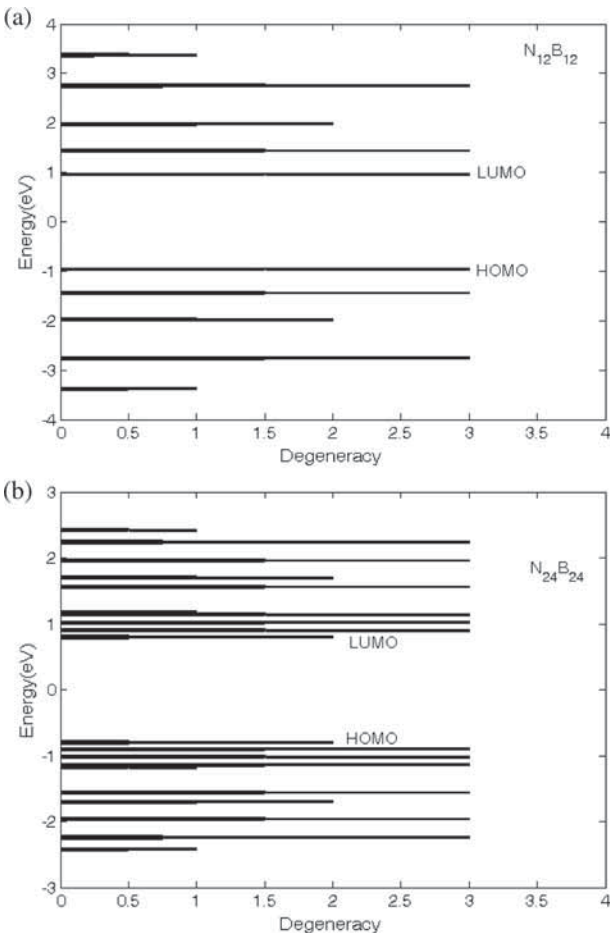

Figure 3. The degeneracy of (**a**) $B_{12}N_{12}$ and (**b**) $B_{24}N_{24}$ molecules as a function of energy (eV/t_0).

respectively. The energy gaps of $B_{12}N_{12}$ and $B_{24}N_{24}$ molecules are presented in figures 3a and 3b, respectively. The energy gap and the energy levels in figures 3a and 3b are in good agreement with the results of the B3LYP/6-31G approximation [37].

For $V_b = 0.0$ V and $V_g = 0.0$ V, the transmission spectra of $B_{12}N_{12}$ and $B_{24}N_{24}$ molecular junctions against the electron energy are demonstrated in figures 4a and 4b, respectively. The transmission spectra of

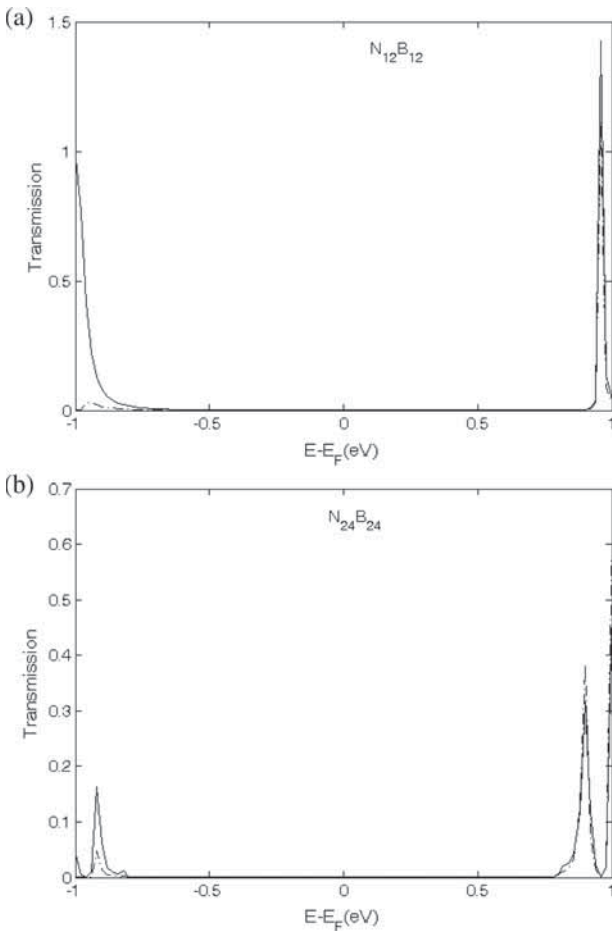

Figure 4. Transmission coefficient (TC) as a function of energy (eV/t_0) for (**a**) $B_{12}N_{12}$ and (**b**) $B_{24}N_{24}$ molecules when $V_b = V_g = 0$. Curves represent the parallel (-) and antiparallel (-·) alignments of the magnetisation of the electrodes.

$B_{12}N_{12}$ and $B_{24}N_{24}$ molecular junctions are plotted for the parallel (-) and antiparallel (-·) configurations. The peaks of the transmission function spectrum are located near the molecular level. In other words, we observe the peaks of transmission when the electron energy of transmitted through the molecule is near to the molecular levels [31]. In figures 4a and 4b, the value of transmission coefficient (TC) near the Fermi energy is zero. In this case, the molecule is in the off-state. Using the gate voltage, the TC values can vary and current can be generated. In other words, the device serves as a conductor and the current increases linearly for a certain gate voltage with the increase in bias voltage.

The transmission spectra of $B_{12}N_{12}$ molecular junction are plotted in parallel (-) and antiparallel (-·) configurations for $V_b = 0.0$ V and $V_g = 0.5$ V (figure 5). Comparing figure 4a with figure 5 reveals the influence of gate voltage on the transmission spectra. Evidently, the positions of transmission peaks against

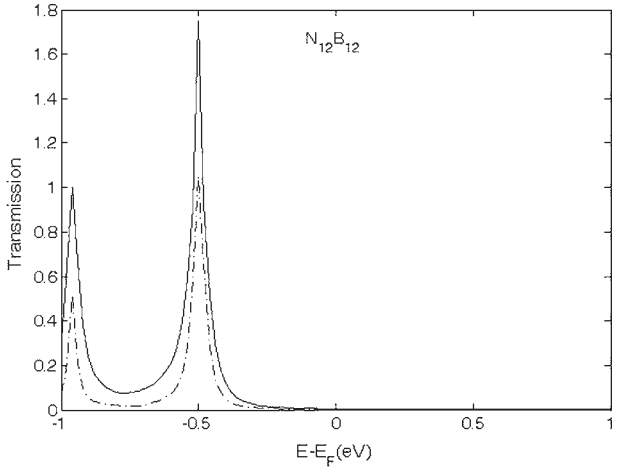

Figure 5. TC as a function of energy (eV/t_0) for (**a**) $B_{12}N_{12}$ molecule when $V_b = 0.5$ V and $V_g = 0.5$ V. Curves represent the parallel (-) and antiparallel (-·) alignments of the magnetisation of the electrodes.

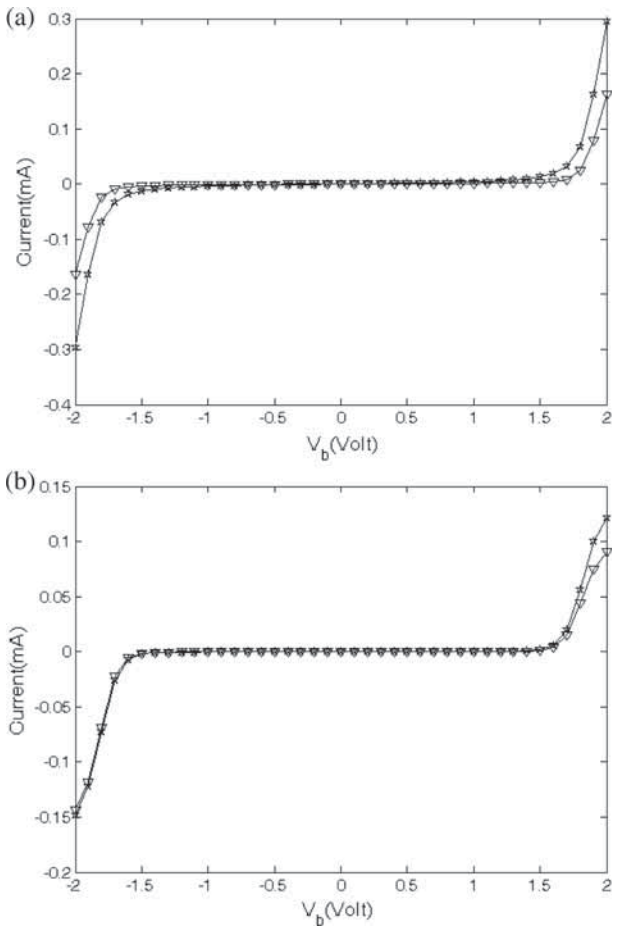

Figure 6. The current–bias voltage characteristics in the parallel (∗) and antiparallel (△) configurations for (**a**) $B_{12}N_{12}$ and (**b**) $B_{24}N_{24}$ molecules.

energy are moved by the gate voltage, thereby, the energy levels and availability of states around the Fermi energy change by the gate voltage. Therefore,

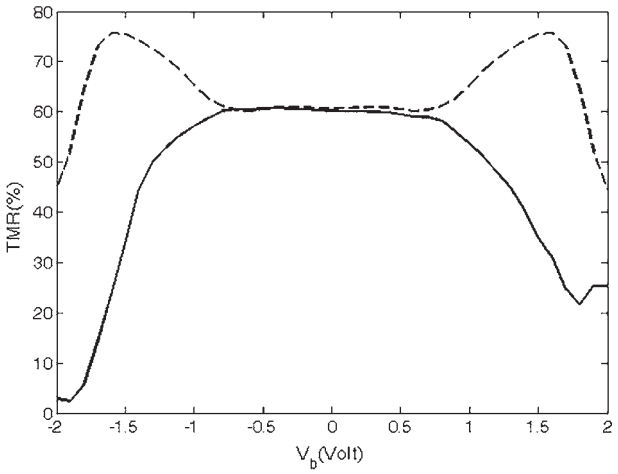

Figure 7. The TMR ratio as a function of bias voltage for the $B_{12}N_{12}$ (–) and $B_{24}N_{24}$(--) molecules.

conduction and electron density (resistance) in the molecule change by the gate voltage because they are dependent on the availability of the state around the Fermi energy.

The surface density of states of the spin-up electrons is different from that of the spin-down electrons in the FM electrodes [12]. Considering the quantum tunnelling phenomenon through the molecule, it has been shown that the transmission spectrum for the parallel configuration is different from that of the antiparallel configuration [12]. The origin of this effect is explained in [12].

Figure 6 interprets the current–bias voltage characteristics of B_nN_n molecule in the presence of magnetic field for the parallel (∗) and antiparallel (△) configurations. The step-like behaviour of I–V curves indicates that a new channel is created. The magnitude of the current flowing through the molecule is in the order of milliampere. At low applied voltages (-1 to $+1$ V), the magnitude of the current flowing through the molecule is not visible in the I–V curves. Figures 4 and 5 show that the spectrum of parallel transmission is different from that of antiparallel configuration. Therefore, I_p and I_a are different. The physical behaviour of the I–V curve of the $B_{12}N_{12}$ molecule is similar to that of the $B_{24}N_{24}$ molecule. Figure 6a, in comparison with figure 6b, shows that the current values of $B_{12}N_{12}$ are larger than those of $B_{24}N_{24}$ because the electron wave for the $B_{24}N_{24}$ molecular junction scatters more than the electron wave for the $B_{12}N_{12}$ molecular junction.

The TMRs as a function of applied bias voltage (V_b) are plotted in figure 7 for the $B_{12}N_{12}$ and $B_{24}N_{24}$ molecules. The values of current in the parallel configuration vs. the bias voltages are larger than those in the antiparallel configuration, where the corresponding TMR is positive.

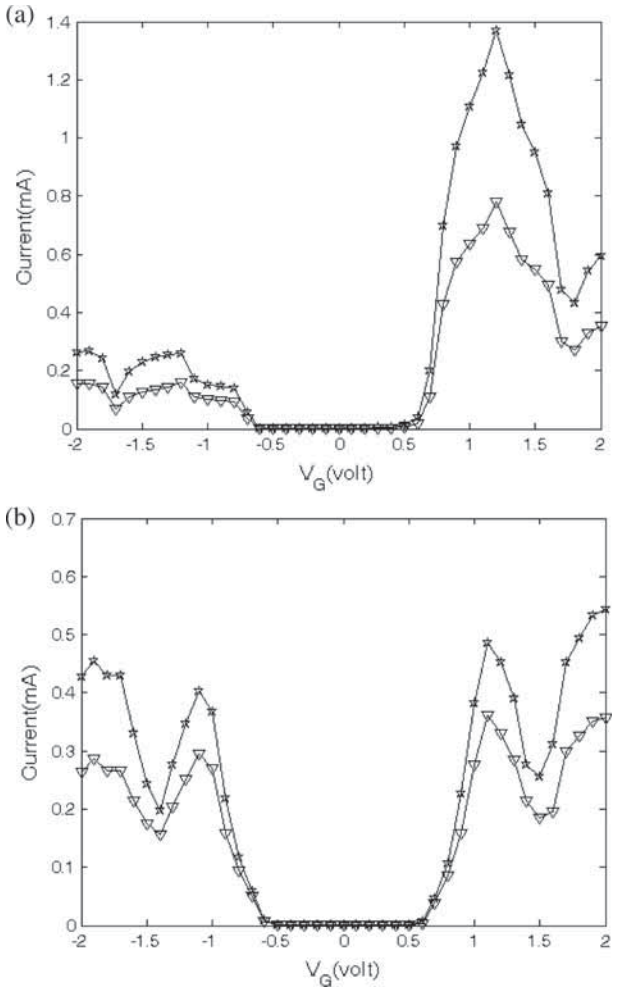

Figure 8. (**a**) The current–gate voltage characteristics in the parallel (∗) and antiparallel (△) configurations for (**a**) $B_{12}N_{12}$ and (**b**) $B_{24}N_{24}$ molecules.

For a $B_{24}N_{24}$ molecule, with a further increase in the applied voltage, the TMR ratio increases and then decreases. This process repeats in a similar way as described in the following. Our results in figure 7 show that the TMR curve of $B_{24}N_{24}$ has peaks at ∼0.0, −2.0 and +1.8 V and has the maximum value (about 60%) at zero bias voltage. The comparison of TMR behaviour of $B_{12}N_{12}$ with TMR behaviour of $B_{24}N_{24}$ shows that a peak of TMR for $B_{12}N_{12}$ occurs at zero bias voltage similar to the TMR of $B_{24}N_{24}$. Three peaks are observed in the TMR curve of $B_{12}N_{12}$. In addition, the maximum values of TMR for $B_{12}N_{12}$ (i.e., 75%) are seen at voltages −1.6 and +1.6 V. The results indicate that the decrease in the B–N fullerene size increases the maximum value of TMR. Moreover, it shifts the maximum value of TMR to a higher voltage. Figure 7 shows that the TMR of $B_{24}N_{24}$ for low bias voltage is almost the same as the TMR of $B_{12}N_{12}$. The TMR of B–N fullerene first decreases with a further increase in the applied

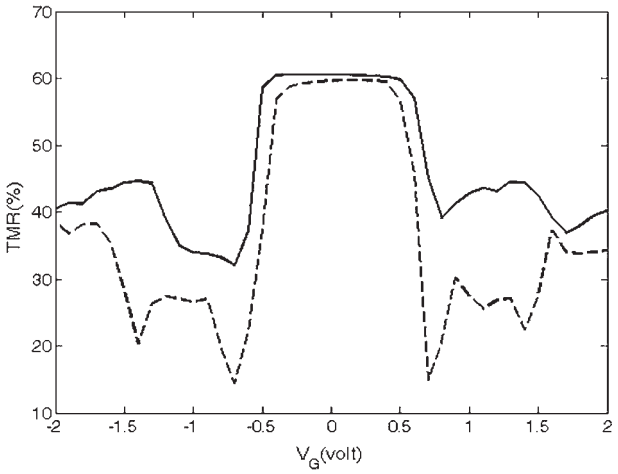

Figure 9. The TMR ratio as a function of gate voltage for $B_{12}N_{12}$ (–) and $B_{24}N_{24}$(--) molecules.

voltage. Thus, our calculations are in agreement with similar systems [10].

Using a similar method, Saffarzadeh [16] reported a maximum value of 60% for C_{60} TMR in low voltages (−0.2 to +0.2 V). In these voltages, the current is invisible. The I–V curve of $B_{12}N_{12}$ compared with C_{60} indicates that the fullerene-like alternate BN cages increase current, with three orders of magnitude [16,33]. Moreover, the maximum value of $B_{12}N_{12}$ TMR ratio is 25% bigger than that of C_{60}. The current value of $B_{12}N_{12}$ is visible when the TMR value has its maximum [16].

To investigate the other features, the effect of the gate voltage on the current of $B_{12}N_{12}$ and $B_{24}N_{24}$ molecules is plotted in figures 8a and 8b when $V_b = 0.5$ V. First, the current is invisible at a low applied voltage (−0.5 to +0.5 V). Increasing the gate voltage up to $V_g = \pm$ 0.5 V, the current follows through molecules. Evidently, the current increases significantly when the transmission peak moves to the bias window by the change in the gate voltage.

In figure 9, TMR vs. V_g curves are shown for $B_{12}N_{12}$ and $B_{24}N_{24}$ molecules. When V_g is applied, the number of peaks increases and the maximum values of the TMR vary. In order to control the electron density and resistance in the device, the gate voltage is used. When the gate voltage increases, the highest occupied molecular orbital (HOMO) or the lowest unoccupied molecular orbital (LUMO) peak moves to the energy window region. In such a condition, the current flows through resonant tunnelling.

4. Conclusion

The spin-dependent carrier transport in a molecular junction consisting of $B_nN_n(n = 12, 24)$ cages coupled

to two ferromagnetic leads was investigated using the Landauer formula based on the NEGF method. First, the transmission spectra of B_nN_n molecular junctions were calculated for the parallel and antiparallel configurations. These spectra are important for the study of transport properties of molecules. Then, we calculated the current–bias (gate) voltage characteristics of B_nN_n molecule. The TMRs, as a function of the applied bias and gate voltages, were explored for the mentioned molecules. The spin-dependent transport properties of the $B_{12}N_{12}$ molecule were compared with those of the $B_{24}N_{24}$ and C_{60} molecules.

References

[1] S Ikeda, J Hayakawa, Y Ashizawa, Y M Lee, K Miura, H Hasegawa, M Tsunoda, F Matsukura and H Ohno, *Appl. Phys. Lett.* **93**, 082508 (2008)

[2] M Ouyang and D Awschalom, *Science* **301**, 1074 (2003)

[3] N Aoki, R Brunner, A M Burke, R Akis, R Meisels, D K Ferry and Y Ochiai, *Phys. Rev. Lett.* **108**, 136804 (2012)

[4] H Dalgleish and G Kirczenow, *Phys. Rev. B* **73**, 235436 (2006)

[5] B Wang, Y Zhu, W Ren, J Wang and H Guo, *Phys. Rev. B* **75**, 235415 (2007)

[6] S Joo *et al*, *Appl. Phys. Lett.* **100**, 172406 (2012)

[7] Z H Xiong, D Wu, Z V Vardeny and J Shi, *Nature* **427**, 821 (2004)

[8] M Jullière, *Phys. Lett. A* **54**, 225 (1975)

[9] T Miyazaki and N Tezuka, *J. Magn. Magn. Mater.* **139**, 231 (1995)

[10] J S Moodera, L R Kinder, T M Wong and R Meservey, *Phys. Rev. Lett.* **74**, 3273 (1995)

[11] http://www.MRAM-info.com/

[12] I Zutic, R Oszwaldowski, J Lee and C Gothgen, *Spintronics handbook: Spin transport and magnetism* edited by E Y Tsymbal and I Zutic (CRC Press, New York, 2011)

[13] B Elsafi and F Trigui, *Ind. J. Phys.* **90**, 35 (2016)

[14] T Oku, T Hirano, M Kuno, T Kusunose, K Niihara and K Suganuma, *Mater. Sci. Eng. B* **74**, 206 (2000)

[15] H Zare-Kolsaraki and H Micklitz, *Eur. Phys. J. B* **40**, 103 (2004)

[16] A Saffarzadeh, *J. Appl. Phys.* **104**, 123715 (2008)

[17] K Yoshida, I Hamada, S Sakata, A Umeno, M Tsukada and K Hirakawa, *Nano Lett.* **13**, 481 (2013)

[18] X Fei, G Wu, V Lopez, G Lu, H.-J Gao and L Gao, *J. Phys. Chem. C* **119**, 119(2015)

[19] D L Strout, *J. Phys. Chem. A* **105**, 261 (2001)

[20] O Stéphan, Y Bando, A Loiseau, F Willaime, N Shramchenko, T Tamiya and T Sato, *Appl. Phys. A* **67**, 107 (1998)

[21] D L Strout, *Chem. Phys. Lett.* **383**, 95 (2004)

[22] R R Zopea, T Barua, M R Pederson and B I Dunlapet, *Chem. Phys. Lett.* **393**, 300 (2004)

[23] H S Wu, X Y Cu, X F Qin and D L Strout, *J. Mol. Model.* **123**, 537 (2006)

[24] S K Gupta, H He, I Lukačević and R Pandey, *Phys. Chem. Chem. Phys.* **19**, 30370 (2017)

[25] Y Egami and H Akera, *Physica E* **88**, 212 (2017)

[26] J Ouyang, M Long, X Zhang, D Zhang, J He and Y Gao, *Comput. Condens. Matter* **4**, 40 (2015)

[27] H R Vanaie and M Yaghobi, *Ind. J. Phys.* **273**, 1 (2017)

[28] S Sanvito, *Nat. Nanotechnol.* **2**, 204 (2007)

[29] W P Su, J R Schrieffer and A J Heeger, *Phys. Rev. B* **22**, 2099 (1980)

[30] S A Ketabi and M Nakhaee, *Pramana – J. Phys.* **86**, 669 (2016)

[31] S Datta, *Electronic transport: Atom to transistor* (Cambridge University Press, New York, 2005)

[32] Y Asai and H Fukuyama, *Phys. Rev. B* **72**, 085431 (2005)

[33] H R Vanaie and M Yaghobi, *Physica E* **60**, 147 (2014)

[34] T Oku, A Nishiwaki and I Narita, *Sci. Tech. Adv. Mater.* **5**, 635 (2004)

[35] G Seifert, P W Fowler, D Mitchell, D Porezag and T Frauenheim, *Chem. Phys. Lett.* **268**, 352 (1997)

[36] T Oku *et al*, *Chem. Phys. Lett.* **380**, 620 (2003)

[37] M Yaghobi and M Yaghobi, *Mol. Phys.* **112**, 206 (2014)